Tribology Online

Japanese Society of Tribologists
http://www.tribology.jp/trol/

Vol. 16, No. 3 (2021) 159-169.
ISSN 1881-2198
DOI 10.2474/trol.16.159

Article

Tribological Behavior of Friction Pairs in a High-Pressure Vane Pump under Variable Working Conditions

Shaonian Li[1)*], Hao Liu[2)], Yi Li[1)], Shangling Bao[1)] and Pan Yang[1)]

[1)] College of Energy and Power Engineering, Lanzhou University of Technology, No.287, Langongping Road, Lanzhou 730050, China
[2)] School of Marine Science and Technology, Northwestern Polytechnical University, No.127, Youyi West Road, Xi'an 710072, China

*Corresponding author: Shaonian Li (Lsn19@163.com)

Manuscript received 07 April 2021; accepted 10 July 2021; published 31 August 2021

Abstract

The tribological behavior of the friction pairs in a high-pressure vane pump under variable working conditions was experimentally studied; in particular, the effects of the varying sliding velocity (1.45–3.61 m/s) and contact pressure (0.11–0.44 MPa) on the friction coefficient and wear rate of the friction pairs in pumps with and without vanes in the vane slot of rotor were investigated. In both cases, the friction coefficient increased with increasing sliding velocity and decreased when the increase of contact pressure in two cases when the contact pressure is 0.22 MPa. Further, the wear rate decreased with increasing contact pressure. With increasing velocity, the friction coefficient was more influenced by the vane compared with wear rate. The main tribological mechanism of wear surface of the valve plate is mechanical ploughing. At a sliding velocity of 2.89 m/s, both with and without vanes, increasing the contact pressure resulted in a reduced friction coefficient and enhanced wear rate. When the contact pressure increased, the vane did not significantly influence the friction coefficient and wear rate. During this time, the wear surface morphology of the valve plate exhibited mainly mechanical plowing and adhesion wear marks.

Keywords

vane pump, friction pairs, friction coefficient, wear rate, wear morphology

1 Introduction

Vane pumps are advantageous owing to features such as small overall dimensions, compact structure, uniform flow, stable operation, low noise, and long service life. They have various applications, such as in machine tools, metallurgy, and injection molding machines [1-5]. There are three friction pairs in a vane pump: the sliding friction of the rotor on the valve plate surface, that of the vane sliding in the radial direction in the vane slot of rotor, and that of the vane top scraping the stator's inner surface in the circumferential direction [6-10]. With the development of high-pressure vane pumps, an increase in the working pressure or rotating speed will have different effects on the friction and wear morphology of these friction pairs [11-14]. Increasing the fluid pressure in the oval oil chamber of the intra-vane increases the contact force when the vane tip slides on the stator's inner surface. Excessive scraping force will induce vane deformations and fractures and produce vibration scratches on the inner surface of the stator. The telescopic motion of the vane in the vane slot of rotor will cause the wear of its side in contact with the slot and reduces its thickness. Despite the good tribological characteristics of the valve plate and rotor, increasing the oil pressure enhances the compression force between them, leading to rapid wear on the contact surfaces [15-18]. Vane pumps often exhibit valve plate wear phenomenon in actual use. The rotor is found too often induce scratches on the surface of the failed valve plate, and the copper plating falls off owing to adhesion wear when the valve plate is considerably worn.

The research on the vane pump friction pairs has yielded the following results: Zhao et al. [19] have formulated the pressure–flow characteristic equation of the pressure-limiting variable vane pump and pointed out that friction resistance would cause its hysteresis; they experimentally confirmed that the loading and unloading curves of the pump do not coincide because of friction resistance.

Chen et al. [20] investigated the vane pump material and discovered the reason for its wear failure. According to the results of microstructure and hardness analysis indicated that the working environment and structure of a two-vane pump greatly influence the failure form of the vane pump material; in addition, they suggested that the depth of the nitriding layer and vane hardness should be optimized in terms of processing technology and materials.

Li et al. [21] experimentally studied the influence of rotation speed on the friction characteristics of the valve plate friction

pair in a vane pump and concluded that with increasing rotational speed, the friction coefficient increased and wear rate decreased.

Currently, through the research on and advances in the vane pump design and manufacture, the performance, working pressure, and service life of vane pumps have been greatly improved [22-27]. However, few studies on the friction and wear of the vane, rotor, and valve plate in terms of tribological behavior exist. An investigation of the tribological characteristics of the friction pairs in high-pressure vane pumps could significantly contribute to their design optimization and performance and service life improvement [28-30]. A set of friction and wear test system was innovatively designed to simulate the operation of vane pump in this paper, mainly analyzed the wear mechanism and failure forms of the valve plate under variable working conditions, such as the sliding speed and the contact pressure of the rotor and the valve plate, which provided a theoretical basis for the development of vane pump to high speed and high pressure.

2 Friction test on the vane pump friction pairs

2.1 Test model

The test object was 25VQ21 double-acting vane pump, and it's theoretical flow rate was 67.5 mL/r, the maximum rotation speed and working pressure was 2500 r/min and 21 MPa, the structure diagram of the pump as show in Fig. 1. The "I", "II" and "III" marked on the surface of the valve plate in Fig. 1 are respectively the damping groove for the bottom cavity of the vanes, the damping groove for the middle cavity of the main vanes and small vanes, the oil discharge ports. The test model of the vane pump was designed to simulate the working conditions of a real vane pump. To observe the internal structure of the vane pump, a semi-transparent shell was utilized. The test model, valve plate, rotor, and vanes are as shown in Fig. 2. A sealing gasket was installed between the top cover and the pump case, which was pressed by four hexagon bolts to avoid oil leakage from the gap. In addition, the using of the skeleton seal ring solved the problem of oil leakage from the gap of the pump shaft and the top cover during the shaft was rotating. The test model was placed on the friction testing machine; its main shaft was connected to the pump shaft. The rotor was driven by the pump shaft, and its outer ring was equipped with a stator. A valve plate was installed on the lower side of the stator. When the rotor was moved by the shaft, the three friction pairs were formed.

In the selection of materials of friction pairs, bronze and steel are a pair of typical antifriction materials, which have good wear resistance performance. Therefore, this paper used the valve plate coated with bronze layer and the rotor, stator, vanes made of steel as friction pair materials. The contour arithmetic mean deviation (Ra) is usually used to characterize the surface roughness and represents the micro unevenness. In this paper, the contour arithmetic mean deviation of each part was Ra = 0.8 μm. The rotor, stator, vanes, and valve plate were made of 20CrMnMo steel, the valve plate surface in contact with the

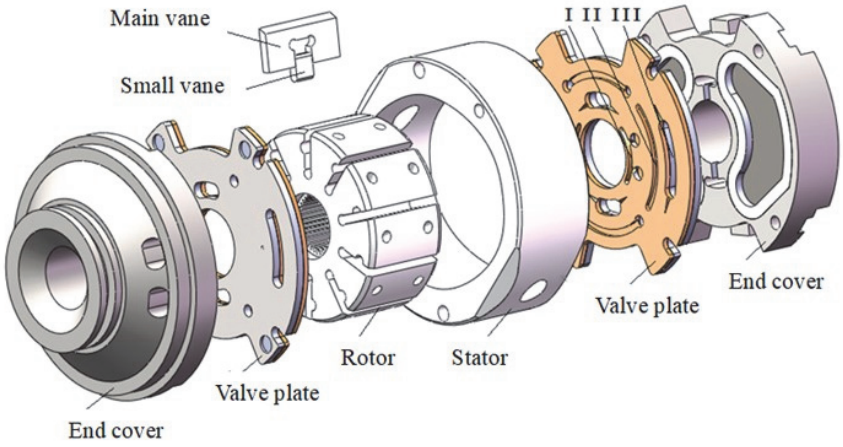

Fig. 1 Structure diagram of double-acting vane pump

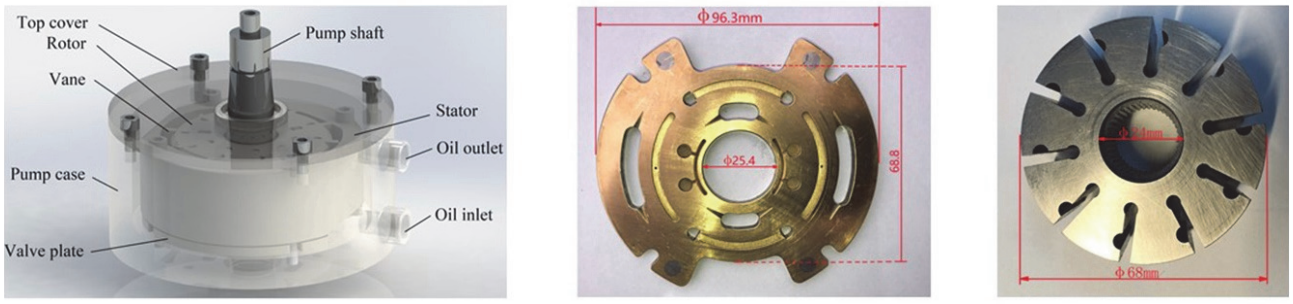

(a) (b) (c)

Fig. 2 Test model of the vane pump and it's parts
(a) Test model of the vane pump (b) Valve plate (c) Rotor

rotor was plated with a 0.5-mm-thick layer of CuPb10Sn10 bronze, the surface bronze of valve plate is usually processed by electroplating and thermal spraying. Therefore, the friction and wear test was actually the test of rotor, stator and vanes of 20CrMnMo material and that of valve plate of CuPb10Sn10 material, the main physical properties of these alloys are summarized in Table 1.

2.2 Test principle

A friction and wear test system was designed (Fig. 3); it mainly comprised an double-acting vane pump test model, a vertical friction and wear tester, a small hydraulic station, and a data acquisition computer.

The working principle of this tester is schematized in Fig. 4. The shaft of the testing machine was connected to the rotor of the double-acting vane pump; thus, the rotor moved at a certain speed and the shaft speed was detected and adjusted using the rotational speed sensor. The pump case and valve plate were fixed to the guide shaft. The force sensor was placed against the lower end of the connecting shaft of the vane pump and could be lifted and lowered by manually rotating the screw shaft. The torque sensor was mounted on the connecting shaft for detecting the friction torque between the friction pairs. The collected shaft speed, test force, and friction torque data were transmitted to the data acquisition computer and processed in real time.

Table 1 Main physical properties of 20CrMnMo and CuPb10Sn10

Property	20CrMnMo	CuPb10Sn10
Tensile strength (MPa)	1180	250
Yield strength (MPa)	885	230
Elongation (%)	10	64
Shrinkage (%)	45	50
Impact toughness (J)	55	178
Brinell hardness (HBS)	217	75
Modulus of elasticity (GPa)	210	108
Poisson ratio	0.3	0.35

Fig. 3 Friction and wear test system

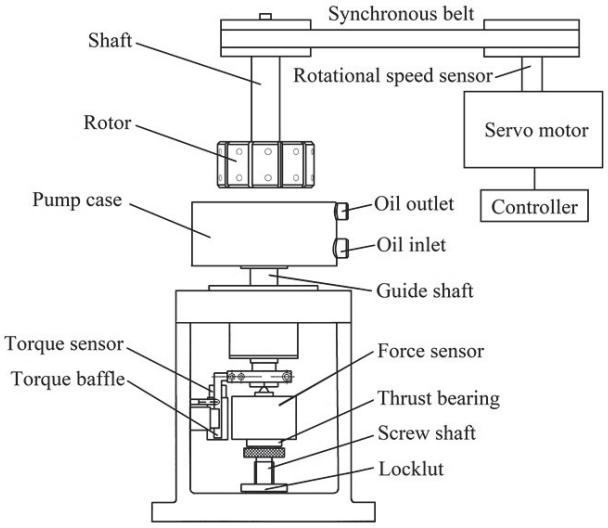

Fig. 4 Working principle of the friction testing machine

A small hydraulic station (Fig. 5) was designed to prevent the adverse influence of high temperature on the experimental process; it could supply the oil pressure for the vane pump and dissipate the heat of the oil. The oil circulated from the hydraulic station to the test model from bottom to top.

For comparability purposes, the friction and wear tests were conducted under two conditions: with and without vanes installed in the vane slot of rotor; the change curves of the friction coefficient thus obtained were measured separately. The value obtained in the case without installed vanes indicates the friction coefficient of the rotor–valve plate friction pair; the value obtained in the case with installed vanes is the comprehensive friction coefficients of the rotor–valve plate, rotor–vane, and vane–stator friction pairs, which refers to the overall effect of the interaction between friction pairs.

The friction coefficient f and wear rate w_s were calculated using Eqs. (1) and (2), respectively:

$$f = \frac{T}{RN} \tag{1}$$

and

$$w_s = \frac{\Delta m}{2\times 60\pi r n \rho N} \tag{2}$$

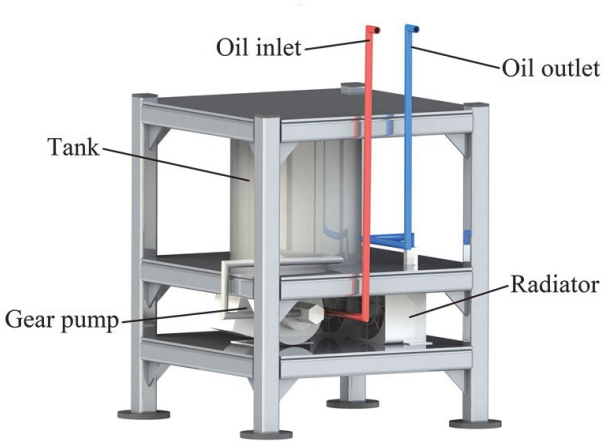

Fig. 5 Hydraulic station

Where f is the friction coefficient of friction pairs; w_s is the wear rate of the valve plate ($\times 10^{-8}$ mm^3/Nm); T is the friction torque measured by the friction torque sensor (N·m); R is the friction radius corresponding to the friction torque (m), R = 0.023 m; N is the loading force (N), N = 200 N, 400 N, 600 N, 800 N; Δm is the wear weight (mg); r is the average radius of the rotor in contact with the valve plate (mm), r = 0.023 m; n is the shaft speed of the friction tester (r/min), n = 600 r/min, 900 r/min, 1200 r/min, 1500 r/min; and ρ is the density of bronze coating on the valve plate (mg/mm^3), ρ = 8.9 mg/mm^3.

The sliding velocity v and contact pressure σ were given by Eqs. (3) and (4), respectively:

$$v = \frac{2\pi rn}{60\times1000} \tag{3}$$

and

$$\sigma = \frac{N}{S} \times 10^{-6} \tag{4}$$

Where v is the sliding velocity of the rotor relative to the valve plate surface (m/s); σ is the contact pressure between rotor and valve plate (MPa); and S is the contact area (m^2), S = 1.818 $\times 10^{-3}$ m^2. The contact area S is the area of the yellow shadow as shown the Fig. 6 when the rotor is installed vane or not.

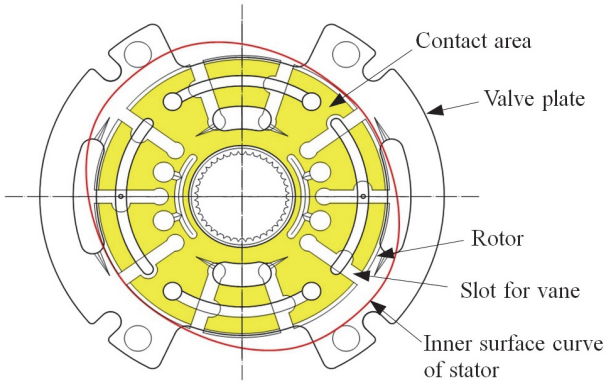

Fig. 6 Schematic diagram of contact area of rotor-valve plate friction pair

The tests were conducted at a sliding velocity of 1.45–3.61 m/s, a contact pressure of 0.11–0.44 MPa, ambient temperature approximately 20°C, and relative humidity of 50% ± 5%. The No. 46 anti-wear hydraulic oil was used for the experiments. Each friction pair was tested continuously for 60 minutes to obtain a steady friction coefficient, and the algebraic average value of the friction coefficient was considered as the average friction coefficient. Subsequently, the mass loss of the valve plate was measured using an electronic balance with an accuracy of 0.1 mg. The wear surface morphology of the valve plate was analyzed using an optical microscope.

3 Experimental results

3.1 Friction coefficient of friction pairs at different sliding velocities and contact pressures

Figure 7 shows the variation curves of the friction coefficient at different sliding velocities and a contact pressure of 0.22 MPa. The friction coefficient curve of the rotor–valve plate friction pair without installed vanes is shown in Fig. 7(a), and the comprehensive friction coefficient curve with installed vanes is shown in Fig. 7(b).

For the rotor–valve plate friction pair, the curve tended stabilize over time (Fig. 7(a)), when the contact pressure is 0.22 MPa and without installed vanes, indicating no obvious running-in process of the friction pair during grinding probably because this pair had good tribological behavior and quickly entered a good friction state. In addition, when the sliding velocity was between 1.45 and 3.61 m/s, an oil film of a certain thickness was formed between the rotor and the valve plate, effectively reducing their direct surface contact. Therefore, the friction coefficient of the rotor–valve plate friction pair was low at different sliding velocities. Furthermore, Fig. 7(a) shows that the friction coefficient of the rotor–valve plate friction pair gradually increased with increasing sliding velocity in the absence of installed vanes; this may be because the sliding speed of the rotor relative to the valve plate was low when the rotating speed is low and the heat caused by friction was small. The hydraulic station continuously injected the cooled oil into the oil chamber of the vane pump. The increase in temperature due to friction was insufficient to increase the vane pump temperature so that the pump operates at a relatively stable

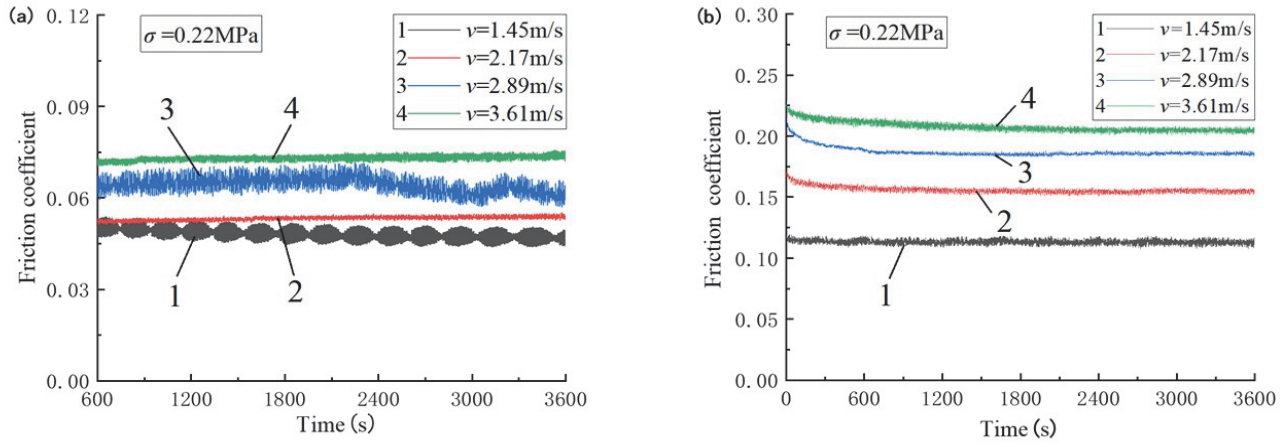

(a) Without installed vanes (b) With installed vanes

Fig. 7 Variation curves of the friction coefficient at different sliding velocities
(a) Without installed vanes (b) With installed vanes

temperature; therefore, the friction coefficient of the rotor–valve plate friction pair was relatively small when the sliding velocity was low. However, as the sliding velocity increased, the instantaneous heat generated by friction could not be dissipated in time, resulting in an increasing-friction-coefficient trend.

The change rule for the friction coefficient shown in Fig. 7(b) is the same as that shown in Fig. 7(a): The comprehensive friction coefficient increased with increasing sliding velocity but its rate of increase was higher in cases wherein the vanes were installed compared with when the vanes were not installed. The friction test with installed vanes yielded a higher change rate of the friction coefficient than that without installed vanes. In Fig. 7(b) the running-in process of the rotor-valve plate friction pair was not too obvious when the sliding velocity was 1.45 m/s. Signs of running-in process could be observed at higher sliding velocities (2.17, 2.89, and 3.61 m/s), but the running-in process was relatively short and the friction pair quickly passed through the running-in process into a state of normal wear.

This can be interpreted as follows: when installed vanes are present, the friction coefficient represents the comprehensive friction coefficient. This comprehensive friction coefficient was larger than that in the case without installed vanes because it included two other friction pairs: the rotor-valve plate, and vane–stator friction pair. The increase in the comprehensive friction coefficient was mainly due to the scratching of the inner surface of the stator during the circular motion of the vane; the vane scraped the inner surface of the stator mainly because the acceleration of radial telescopic of the vane in the vane slot of rotor increases with faster rotor motion, leading to increased centrifugal force of the vane. Furthermore, the existence of the inner curve of the stator accelerated the radial telescopic of the vane, increasing the probability of the vane striking the inner surface of the stator. Therefore, the comprehensive friction coefficient increased.

To better understand the variation of the friction coefficient in the two cases, the friction coefficient variation curves (Fig. 7) were further analyzed. Consequently, the relationship between the friction coefficient and sliding velocity was obtained, as shown in Fig. 8.

In the two cases, the average friction coefficient increased gradually with increasing sliding velocity. This increase was relatively faster in the cases with installed vanes than without

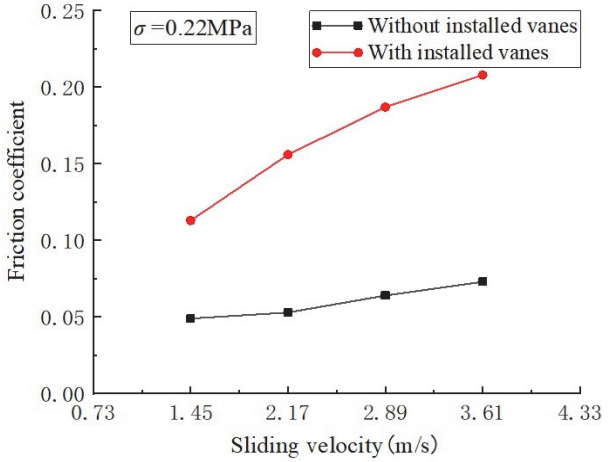

Fig. 8 Friction coefficient variation as a function of the sliding velocity at a contact pressure of 0.22 MPa

installed vanes. This indicates that the proportion of the friction generated by the vane striking the inner surface of the stator gradually increased with increasing sliding velocity. The main proportion of friction and wear are gradually shifted from the rotor–valve plate friction pair to the vane–stator friction pair. Therefore, during the pump operation at medium and low rotational speeds, the friction wear mostly occurred on the surface of the valve plate; additionally, friction and wear to the inner surface of the stator owing to the vane gradually increased with the increasing shaft speed of vane pump.

Figure 9 illustrates the variation curves of the friction coefficient at different contact pressures at a sliding velocity of 2.89 m/s. In the case without installed vanes, the average friction coefficient reached 0.11 when the contact pressure was 0.11 MPa, which is at a higher level than the other pressure conditions (Fig. 9(a)). Curve 1 shows a significant downward trend and starts to stabilize after approximately 30 min, indicating that the friction pair has a clear running-in process at a contact pressure of 0.11 MPa. When the contact pressure further increased, the running-in time gradually decreased; at 0.44 MPa contact pressure, as showed in Curve 4, the average friction coefficient was only approximately 0.043. The running-

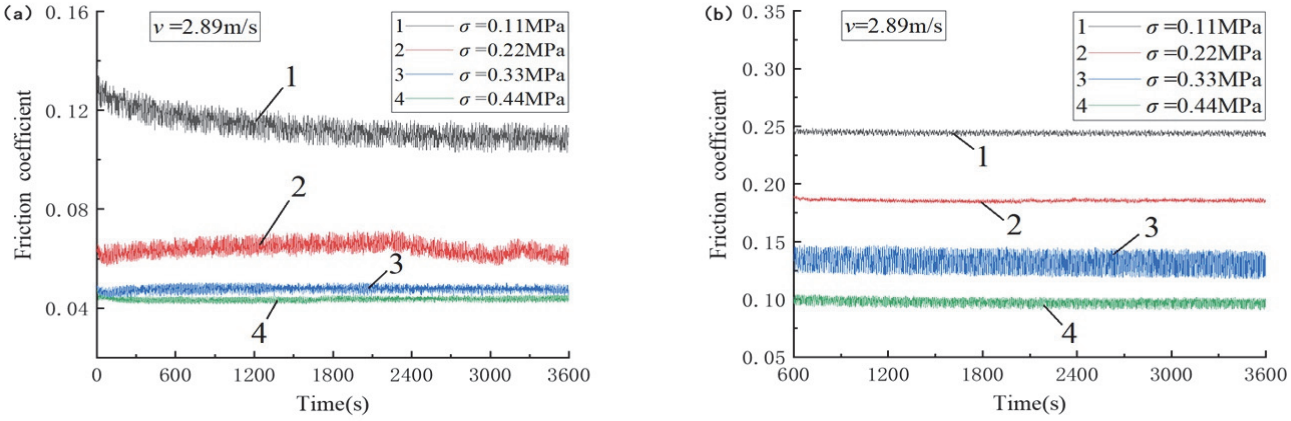

(a) Without installed vanes (b) With installed vanes

Fig. 9 Variation curves of the friction coefficient at different contact pressures
(a) Without installed vanes (b) With installed vanes

in period of the rotor and valve plate was approximately 10 min, which significantly lower than that shown in Curve 1. Thus, when the sliding velocity was 2.89 m/s, the running-in period of the rotor–valve plate friction pair decreased as the contact pressure increased.

Figures 9(a) and (b) both show that friction coefficient decreased with increasing contact pressure. The friction and wear mechanism is analyzed as follows. When the contact pressure is low, the rotor and valve plate surfaces are not smooth or flat, the surfaces of the two friction pairs exhibit irregular micropeaks. The initial contact between the two surfaces exhibits a higher micropeak during the friction pair relative movement and the valve plate exhibits the state of furrow wear. Although the micropeak with high hardness can reduce the micropeak with low hardness, the low contact pressure prevents this from occurring. The micropeaks of the two microsurfaces exist for a long time when the contact pressure is low and the friction coefficient increases macroscopically. Upon increasing the contact pressure, the larger micropeak of the valve plate surface is cut off and the number of micropeaks is reduced, leading to the continuous reduction of the surface roughness and the friction coefficient. The number of micropeak contacts increased with increasing contact pressure, as the micropeaks continued to be cut, the valve plate surface became smoother and the fluid dynamic pressure lubrication was more likely to occur on this surface. In addition, the presence of an oil film reduced the direct contact between the contact surfaces, thereby decreasing the friction coefficient.

Figure 10 shows the relationship between the friction coefficient and contact pressure in the two tested cases at a sliding velocity of 2.89 m/s. In the cases with and without installed vanes, the friction coefficient decreased when raising the contact pressure, and these parameters exhibited a trend of positive relationship and the curves becomes steeper when the contact pressure was changed from 0.11 to 0.33 MPa, it was indicated the friction coefficient of the friction pair was greatly affected by the contact pressure. This shows that under a light load, the contact pressure has a significant influence on the friction coefficient of the friction pair regardless of the presence of installed vanes. However, under heavy loads, the contact pressure has little effect on the friction coefficient of the friction pair. In this regard, the difference value between the friction coefficient curves in the cases with and without installed vanes represents the comprehensive result influenced by the vane-stator friction pairs. And the difference value mainly caused by the scraping friction of the vane on the inner surface of the stator.

In addition, the friction coefficient for the vane–stator friction pair gradually decreased as the contact pressure increased; further, the friction coefficient variation decreased with increasing contact pressure. Furthermore, the larger the contact pressure is, the smaller the change range of friction coefficient is. Therefore, the influence of the vane-stator friction pair on the comprehensive friction coefficient decreased as the contact pressure increased, consequently, the proportion of vane-stator friction pair taken up with comprehensive friction coefficient became smaller.

3.2 Wear rate of valve plate under different sliding speeds and contact pressures

Figure 11 illustrates the effect of the sliding velocity on the wear rate of the valve plate at a contact pressure of 0.22 MPa. In the cases with and without installed vanes, the wear rate decreased as the sliding velocity increased: when the sliding velocity changed from 1.45 to 2.89 m/s, the curve was steep and the wear rate decreased rapidly; upon varying the sliding velocity from 2.89 to 3.61 m/s, the curve became gradually gentle and the wear rate decelerated.

The friction mechanism of this phenomenon can be explained as follows. At the same contact pressure, when the sliding speed was low, the residual oil between the contact area of the rotor and the valve plate was easy to be squeezed out, the working condition of the friction pair got worse and tended to be in dry friction state, the poor lubrication condition made the micropeaks on the surface of the valve plate easier to be cut down, which increased the wear rate of the valve plate. Because the material of rotor is relatively harder than that of the valve plate, the cutting effect of the micropeak on the valve plate surface increased. The micropeak cut from the surface of valve plate fell off as copper scraps; some of these scraps were transferred to other areas on the port plate surface while mostly the rest mixed with the oil. In this case, the wear of the valve plate was large. Enhancing the sliding speed reduced the probability of micropeaks colliding at a certain position

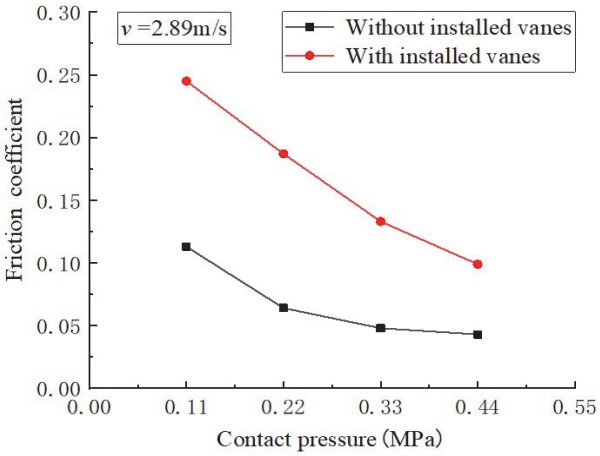

Fig. 10 Friction coefficient variation as a function of contact pressure at a sliding velocity of 2.89 m/s

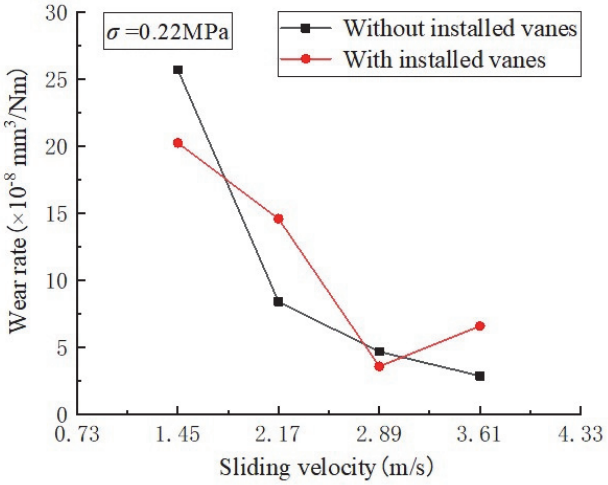

Fig. 11 Wear rate variation as a function of the sliding velocity under a contact pressure of 0.22 MPa

on the two contact surfaces in unit time; fewer copper scraps fell from the valve plate surface and the wear rate of the port plate decreased. This indicates that the wear rate of the valve plate decreases with increasing sliding velocity and is more influenced by a lower sliding velocity. As the sliding velocity increases, the effect of higher sliding velocity on the wear rate tends to decrease. Moreover, at the same sliding velocity and contact pressure, the wear rate values in the cases with and without installed vanes are similar, suggesting that the vane has little effect on the wear rate. The relatively small wear rate of the valve plate (of the order of 10^{-8}) indicates that the rotor and valve plate exhibited good tribological behavior depending on their constituent materials.

Figure 12 shows the wear rate variation curves at different contact pressures for a sliding velocity of 2.89 m/s. The wear rate of the valve plate increased with increasing contact pressure in the friction tests with and without installed vanes. The change rate of the valve plate wear was relatively low when the contact pressure varied from 0.11 to 0.22 MPa, and the wear rate increased faster when the contact pressure changed from 0.22 to 0.44 MPa. This means that when the contact pressure of the rotor–valve plate friction pair is small, the curve growth is gentle and the wear rate of the value plate increases slowly; as the contact pressure increases, the curve becomes steeper and the wear rate of the valve plate increases rapidly. The friction coefficient of the valve plate friction pair decreased with increasing contact pressure, and the wear rate of the valve plate increased. This indicates that a small friction coefficient cannot inhibit the decrease in the wear rate of the friction pair.

The friction mechanism can be explained as follows. A high contact pressure results in large peaks between the two friction pair surfaces being quickly cut off and flowed into the oil. As running-in period occurred of the two surfaces, their surface roughness gradually decreases and the rotor slides more easily on the valve plate surface, the frictional resistance and the friction coefficient decrease. Consequently, more micropeaks fall off the valve plate surface, resulting in an increased wear rate. Under light loads, the rate of micropeaks falling off the valve plate surface is slow and showed a slowly wear rate macroscopically; under heavy loads, the rate of micropeaks falling off the valve plate surface more rapidly and wear rate is higher macroscopically.

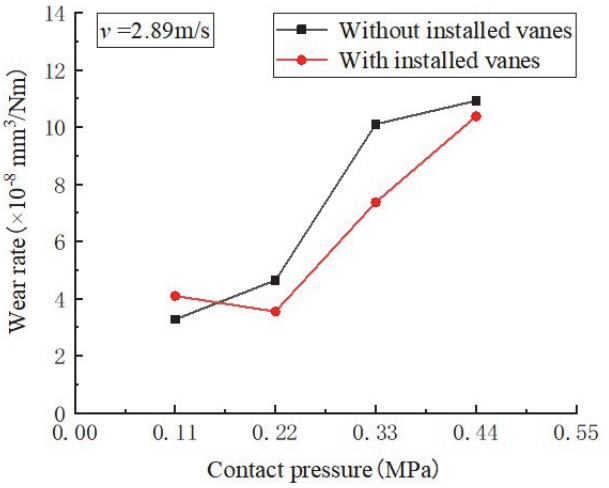

Fig. 12 Wear rate variation as a function of the contact pressure at a sliding velocity of 2.89 m/s

3.3 Wear surface morphology of valve plate

Figures 13–16 display the optical microscopy images of the wear surface marks and tracks after the tests and their variations with varying sliding velocity and contact pressure. Under a fixed contact pressure of 0.22 MPa and without installed vanes (Fig. 13), the valve plate surface appeared glossy with several slight scratches along the circumference when the sliding velocity was 1.45 m/s (Fig. 13(a)); this was due to the slight furrowing effect of the rotor on it. When increasing the sliding velocity (Figs. 13(b)–(d)), the number of scratches gradually increased, but not increased their width, indicating that the sliding velocity increase has little effect on the scratch width. Therefore, the wear surface morphology of the valve plate shown in Fig. 13 was mainly due to the mechanical plowing of the micropeaks on the rotor surface.

Under the same conditions, in the case with installed vanes, the wear was more serious and the valve plate surface exhibited a larger number of scratches with greater width as the sliding velocity increased, as shown in Figs. 14(c)–(d). This can be explained in two ways. First, with the increase in sliding velocity, the vane performs not only radial telescopic motion in the vane slot of rotor but also has an axial vibration impact on the valve plate surface due to mechanical vibration. The instantaneous impact force continuously enhances the width of the scratches on the valve plate surface. Second, the vane may incline out and retract while moving, causing the vane edge to directly strike the valve plate surface and increasing the probability of greater scratch width. Thus, the wear surface morphology of the valve plate in the case with installed vanes revealed mainly mechanical plowing marks.

In the case without vanes at a fixed sliding velocity of 2.89 m/s, a contact pressure of 0.11 and 0.22 MPa resulted in an almost identical number of scratches on the valve plate surface when applying a contact pressure of 0.11 or 0.22 MPa (Figs. 15(a), (b)), but the image for the second case was clearer, indicating larger scratch width. The reason is that the increase in contact pressure between the rotor and valve plate made the micropeak on the rotor sink deeper into the valve plate surface; the rotor slid continuously on the valve plate surface and the micropeak plowed continuously on it, leading to a wider and deeper groove. Figures 15(c) and (d) reveal surface adhesion marks, indicating that the valve plate surface was adhesively worn when the contact pressure is 0.33 MPa. The strong contact pressure cause the material of valve plate surface cannot withstand the strong shearing force from the rotor, consequently, copper is flaked from the surface of the valve plate in some areas. Therefore, when the sliding velocity is 2.89 m/s, the wear surface morphology of the valve plate reveals mainly mechanical plowing marks under light loads; further, it is accompanied by the adhesion wear phenomenon under heavy loads.

Under the same conditions (different contact pressures and a sliding velocity of 2.89 m/s), the presence of installed vanes leads to wider and deeper scratches, as shown by the comparison between Figs. 16(b) and 15(b). In this case, the wide and deep scratches appeared on the valve plate surface when the contact pressure was 0.22 MPa, indicating that the vane exacerbated the wear of the valve plate. Figures 16(b)–(d) clearly illustrate the phenomenon of adhesion wear, the increased probability of adhesive wear on the surface of valve plate due to the presence of the installed vane, and that the wear morphology comprised mainly mechanical plowing and adhesive wear marks. The wear of the valve plate increased

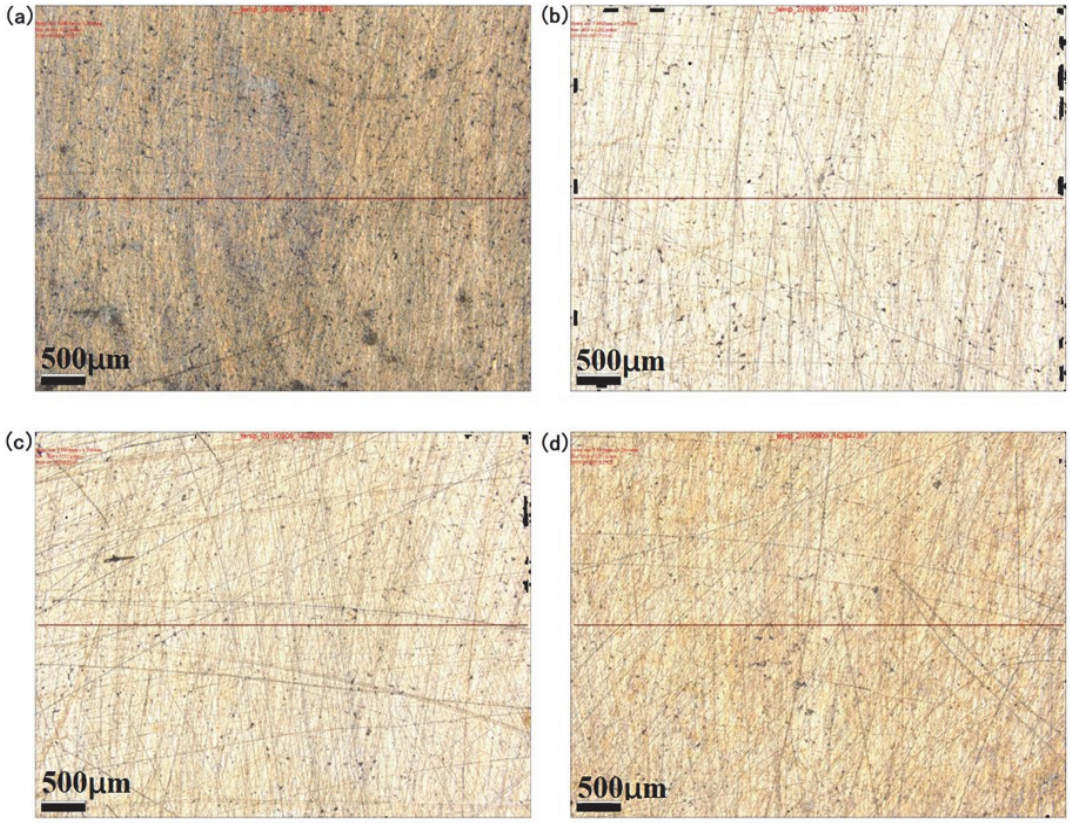

Fig. 13 Wear morphology of the valve plate surface under a contact pressure of 0.22 MPa without vanes and at different sliding speeds. (a) 1.45, (b) 2.17, (c) 2.89, and (d) 3.61 m/s.

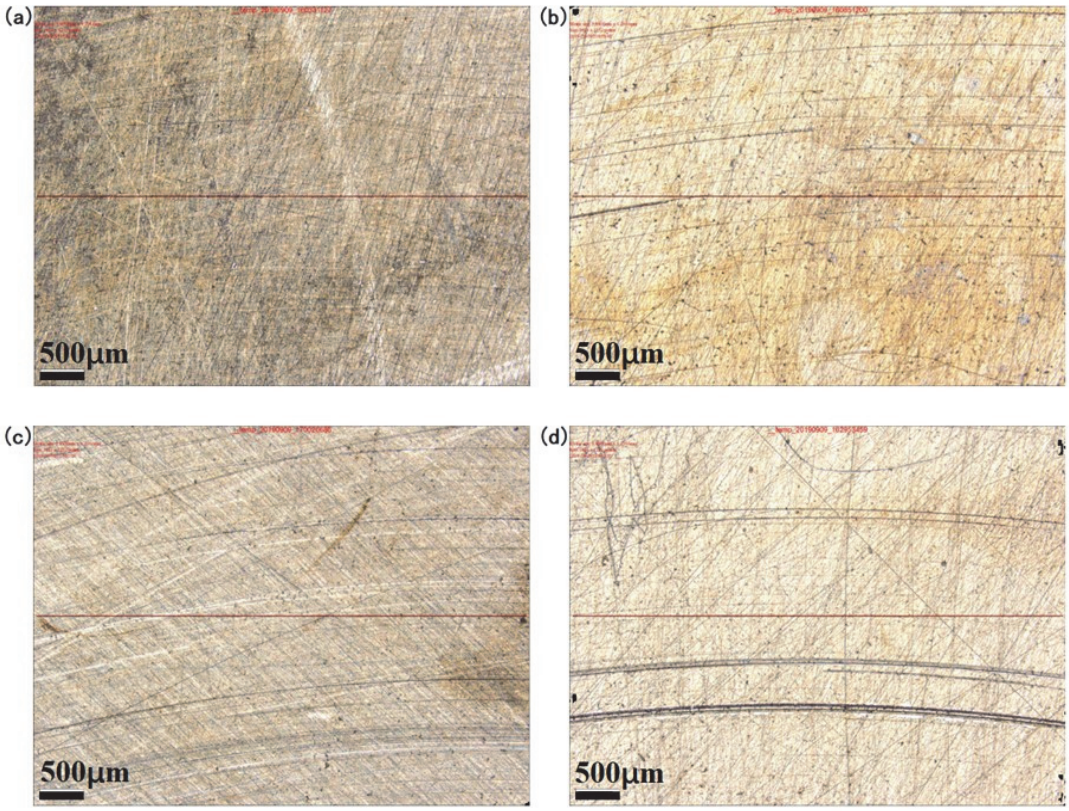

Fig. 14 Wear morphology of the valve plate surface under a contact pressure of 0.22 MPa with installed vanes and at different sliding speeds. (a) 1.45, (b) 2.17, (c) 2.89, and (d) 3.61 m/s.

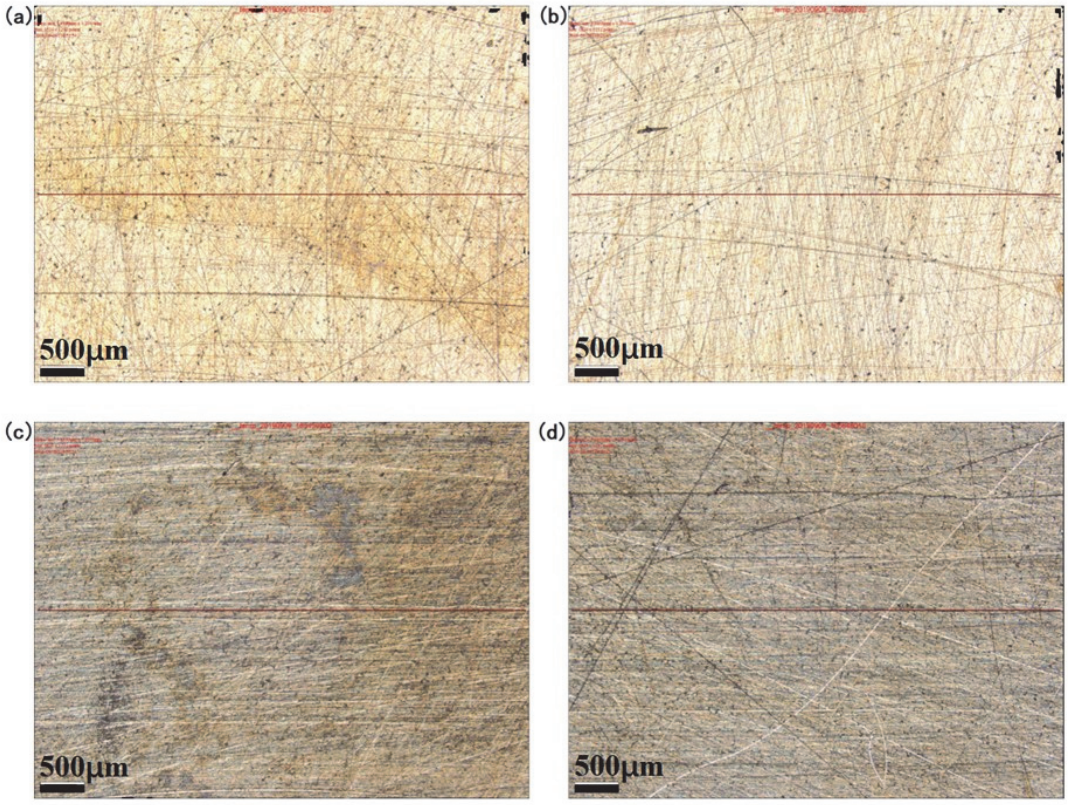

Fig. 15 Wear morphology of the valve plate surface at a sliding velocity of 2.89 m/s without vanes and under different contact pressures. (a) 0.11, (b) 0.22, (c) 0.33, and (d) 0.44 MPa.

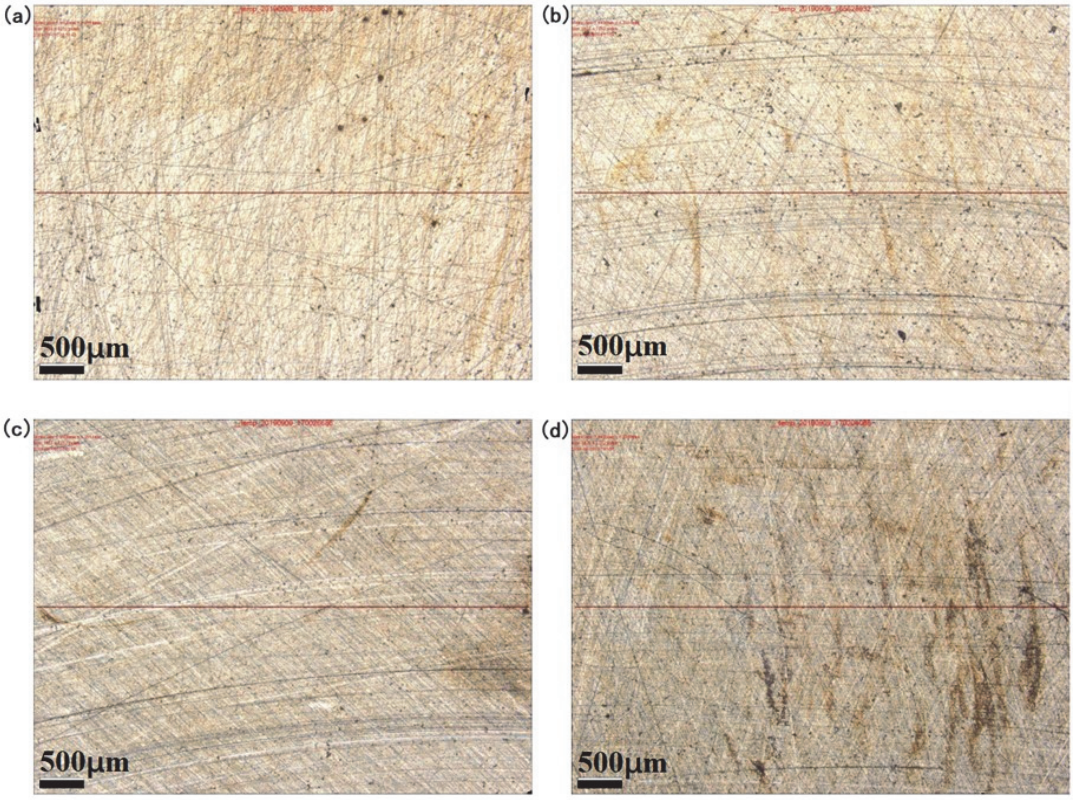

Fig. 16 Wear morphology of the valve plate surface at a sliding velocity of 2.89 m/s, with vanes, and under different contact pressures. (a) 0.11, (b) 0.22, (c) 0.33, and (d) 0.44 MPa.

the frictional power loss and reduced the mechanical and the volumetric efficiencies of the vane pump because of the oil leaking from the scratch groove. Serious wear could make the valve plate undergo plastic deformation and advancing failure, shortening the pump's service life.

4 Conclusions

1) The friction coefficient of the friction pair increased with the increasing sliding velocity in cases with and without vanes when the contact pressure was 0.22 MPa. However, under the same working conditions, this increase was greater and with an obvious but shorter running-in process than in the case without installed vanes. As the sliding velocity increased, the proportion of the wear effect transferred from the valve plate surface to the inner surface of the stator. Regardless of the presence of vanes, the wear rate of the valve plate exhibited a decreasing trend with increasing sliding velocity, the presence of the vanes have little effect on the wear rate.
2) The friction coefficient of the friction pair decreased with increasing contact pressure in cases with and without installed vanes when the sliding velocity was 2.89 m/s. There was a significant running-in process, the duration of which decreased as the contact pressure increases contrast to no installed vanes. Whether or not vanes are installed, the wear rate of the valve plate showed an increasing trend with increasing contact pressure. Increasing the contact pressure leads to a higher wear rate and the vanes have a lower influence on the wear rate.
3) When the contact pressure was 0.22 MPa, the number of scratches on the valve plate surface in the case without installed vanes increased with increasing sliding velocity and the wear surface morphology revealed mainly mechanical plowing marks. The valve plate surface was more worn in the case with installed vanes, and with the increase in the sliding velocity resulted in more scratches with greater width. The wear surface revealed mainly mechanical plowing marks.
4) When the sliding velocity was 2.89 m/s, the valve plate surface exhibited a wide and deep scratch early in the case without vanes; when the contact pressure reached 0.33 MPa, it exhibited adhesive wear marks. The wear occurred mainly via mechanical plowing and adhesive wear. The presence of the vanes exacerbated the wear on the valve plate surface and increased the probability of adhesive wear; the wear morphology revealed mainly mechanical plowing and adhesive wear marks.

Acknowledgments

This work was supported by grants from the National Nature Science Foundation of China (51565026) and Industrial Support and Guidance Project of Colleges and Universities in Gansu Province (2019C-13).

References

[1] Gao, J. F., Sui, G. D., Lv, S. J. and Wen, D. S., "Lubrication Characteristics Analysis of Friction Pairs of Double-Stator Vane Pump Roller Linkages," Journal of Huazhong University of Science and Technology (Natural Science Edition), 47, 5, 2019, 51-55 (in Chinese).

[2] Wang, X. K., Hu, D. F. and Shang, J. D., "Numerical Simulation and Characteristic Analysis of Flow Field in Double-Acting Vane Pump," Hydraulics and Pneumatics, 5, 2013, 23-26 (in Chinese).

[3] Wang, L. L., Zhao, X. T., Guo, S. H. and Wang, M., "Tribological Properties of Surface Microtexture Friction Pairs under Different Lubrication Conditions," Advances in Mechanical Engineering, 11, 10, 2019.

[4] Zhou, P., Liu, R. F. and Zhang, Y., "Vibration Mechanism Analysis and Design Improvement of Blade Pump," Noise and Vibration Control, 32, 2, 2012, 32-33+78 (in Chinese).

[5] Mo, J. T., Gu, C. H., Pan, X. H., Zheng, S. Y. and Ying, G. Y., "Experimental and Numerical Study of the Influence of Loading Direction on the Lubrication and Cooling of Self-Circulating Oil Bearing System Applied in Internal Gear Pumps," Proceedings of the Institution of Mechanical Engineers, Part J: Journal of Engineering Tribology, 232, 4, 2018, 415-426.

[6] Bu, Y. L., Song, Z. P., Yu, G. F., Shan, B. Q., Zhang, Z. G. and Wang, L., "Vane Pump Slide-Wear Issue Optimization Research," Automobile Applied Technology, 14, 2018, 95-97 (in Chinese).

[7] Xu, H. and Jin, H. W., "Leakage and Volumetric Efficiency Experiment of Three-Convex Cam Vane Pump," Hydraulics Pneumatics & Seals, 4, 2018, 26-31 (in Chinese).

[8] Jiang, B. Q., Huang, X., Guo, F., Jia, X. H. and Wang, Y. M., "Effect of Friction Coefficient on the Mixed Lubrication Model of Rotary Lip Seals," Proceedings of the Institution of Mechanical Engineers, Part J: Journal of Engineering Tribology, 234, 11, 2019, 1746-1754.

[9] Ye, C. D., "Discussion on Energy Loss in Vane Pump," General Machinery, 4, 2017, 74-75 (in Chinese).

[10] Wang, Z. R., Ji, H., Hu, Q. H. and Wang, J. S., "Noise Test and Analysis on a Prototype of Electric Motor Pump," Hydraulics Pneumatics & Seals, 9, 2010, 63-65 (in Chinese).

[11] Wen, S. Z., "Progress and Consideration of Lubrication Theory Research," Tribology, 6, 2007, 497-503.

[12] Luo, Y. and Yang, Z. J., "Effect of Different-Condition Parameters on Frictional Properties of Non-Asbestos Phenolic Resin-Based Friction Material," Advances in Mechanical Engineering, 9, 5, 2017.

[13] Truong, D. Q., Ahn, K. K., Trung, N. T. and Lee, J. S., "Theoretical Investigation of a Variable Displacement Vane-Type Oil Pump," Proceedings of the Institution of Mechanical Engineers, Part C: Journal of Mechanical Engineering Science, 227, C3, 2013, 592-608.

[14] Chang, X. D., Peng, Y. X. and Zhu, Z. C., "Tribological Properties of Winding Hoisting Rope between Two Layers with Different Sliding Parameters," Advances in Mechanical Engineering, 8, 12, 2016.

[15] Zhang, Z. H., Nie, S. L., Liao, W. J., Li, L. and Yuan, S. H., "Tribological Behaviors of Carbon Fiber Reinforced Polyetheretherketone Sliding against Silicon Carbide Ceramic under Seawater Lubrication," Proceedings of the Institution of Mechanical Engineers, Part J: Journal of Engineering Tribology, 228, 12, 2014, 1-12.

[16] Cheng, X. R., Dong, F. D., Yang, C. X., Zhao, W. G. and Zhang, N., "The Influence of Particle Diameter on Friction Loss Intensity and Collison Wear Loss Intensity Along Blades of Centrifugal Pump," Journal of Lanzhou University of Technology, 41, 5, 2015, 44-49 (in Chinese).

[17] Huang, A. S., "Treatment of Contact Surface Wear of Engine Crankshaft Oil Seal," Copper Engineering, 4, 2011, 72-73+89 (in Chinese).

[18] Feng, J. J., Zhu, G. J., He, R., Luo, X. Q. and Lu, J. L., "Influence of Wall Roughness on Performance of Axial-Flow Pumps," Journal of Northwest A&F University (Natural Science Edition), 44, 3, 2016, 196-202 (in Chinese).

[19] Zhao, H., Zhu, Y. C., Liu, C. and Hu, X. X., "Research on Friction Characteristic of Pressure-Limiting Variable Vane Pump,"

Manufacturing Technology and Machine Tools, 8, 2008, 129-132 (in Chinese).

[20] Chen, L., Lou, B. Y. and Zheng, X. H., "The Discussion of Lax Cord Protection Mode of Vertical Voluble Hoist Shaft," Coal Mine Machinery, 9, 2004, 40-41 (in Chinese).

[21] Li, S. N., Lin, K. and Liu, H., "Effect of Rotating Speed on Friction Characteristics of Vane Pump Friction Pairs," Hydraulics Pneumatics & Seals, 39, 1, 2019, 53-55 (in Chinese).

[22] Zhang, H. W., "Study of Vane Pump Improvement," Hydraulics and Pneumatics, 8, 2010, 83-85 (in Chinese).

[23] Li, S. N., Wei, L. J., Ji, H., Wang, Z. R. and Na, Y. Q., "Effect of Improved Stator Curve on Characteristic of High-Pressure Intra-Vane Type Pump," Transactions of the Chinese Society for Agricultural, 43, 1, 2012, 219-223 (in Chinese).

[24] Wang, Z. L., WU, Y. C. and Huang, J. H., "The High-Speed Tribological Performance of Port Plates in Axial Piston Pumps," Hydraulics Pneumatics & Seals, 8, 2019, 27-32 (in Chinese).

[25] Li, Y. L., Zhang, F. and Guan, B. W., "Wearing and Failure Analysis of a Hydraulic Piston Pump Plunger," Journal of XIAN Aeronautical University, 37, 1, 2019, 15-21 (in Chinese).

[26] Lin, J., Mou, J. G., Zhang, S. C., Deng, H. Y. and Zhang, S. H., "Analysis and Research on New Type of Double-Acting Contactless Sliding-Vane Pump," Fluid Machinery, 10, 2006, 33-35+70 (in Chinese).

[27] Gao, J. F., Sui, G. D., Lu, S. J. and Wen, D. S., "Lubrication Characteristics Analysis of Friction Pairs of Double-Stator Vane Pump Roller Linkages," Journal of Huazhong University of Science and Technology (Natural Science Edition), 47, 5, 2019, 51-55 (in Chinese).

[28] Uddin, G. M., Khan, A. A. and Ghufran, M., "Experimental Study of Tribological and Mechanical Properties of TiN Coating on AISI 52100 Bearing Steel," Advances in Mechanical Engineering, 10, 9, 2018.

[29] Wang, Z. L., WU, Y. C. and Huang, J. H., "The High-Speed Tribological Performance of Port Plates in Axial Piston Pumps," Hydraulics Pneumatics & Seals, 8, 2019, 27-32 (in Chinese).

[30] Ge, X. Y., "Research of Noise Control on Double-Acting Vane Pump," Machine Tool & Hydraulics, 37, 3, 2009, 87-88+42 (in Chinese).